Available online at www.sciencedirect.com
ScienceDirect
Thin Solid Films 515 (2007) 3507–3512
thin solid films
www.elsevier.com/locate/tsf

Effect of Te additions on the optical properties of (As–Sb–Se) thin films

A.A. Othman [a], K.A. Aly [b,*], A.M. Abousehly [b]

[a] Department of Physics, Assiut University, Assiut, Egypt
[b] Department of Physics, Al Azhar University, Assiut, Egypt

Received 19 February 2006; received in revised form 13 October 2006; accepted 20 October 2006
Available online 1 December 2006

Abstract

Amorphous $(As_{30}Sb_{15}Se_{55})_{100-x}Te_x$ (with $0 \le x \le 12.5$ at.%) were prepared by thermal evaporation. The optical transmission and reflection spectra of these films were measured in the wavelength range of 400–900 nm. The mechanism of the optical absorption follows the rule of allowed non-direct transition. It was found that, the optical band gab E_0 decreases while the width of localized states (Urbach energy) E_c increases by increasing Te content. The relationship between E_0 and chemical composition of the $(As_{30}Sb_{15}Se_{55})_{100-x}Te_x$ system were discussed in terms of Cohesive energy (CE), the average heat of atomization H_s, and the average coordination number N_r. The later are computed from the heat of atomization and the coordination number of used elements, respectively.

Keywords: Physical properties; Optical properties; Glass transition; Crystallization from melt

1. Introduction

Chalcogenide glassy semiconductors have received great attention because of their important optical applications in the infrared region [1,2]. The common feature of these glasses is the presence of localized state in the mobility gap as a result of the absence of long-range order as well as various inherent defects. Investigation of electron transport in disordered systems has been gradually developed and the investigation of gap states is of particular interest because of their effect on the electrical properties of semiconductors [3].

A number of papers [4–11] have appeared in the literature reporting the electrical properties, photoconductivity, glass formation, structure and crystallization kinetics of the As–Sb–Se glasses. Tellurium addition to the later glasses would be expected to decrease their glass transition temperature and reduce their thermal stabilities [12]. According to Kastner [13], the addition of an element with a higher electropositive character than the elements in the host material will tend to decrease the activation energy of the electrical conductivity.

In the present work, the effect of addition of Te ($x=0$, 2.5, 5, 7.5, 10, and 12.5 at.%), which is the highest atomic weight (more electropositive), on the optical properties of the $(As_{30}Sb_{15}Se_{55})_{100-x}Te_x$ is investigated. All measurements were

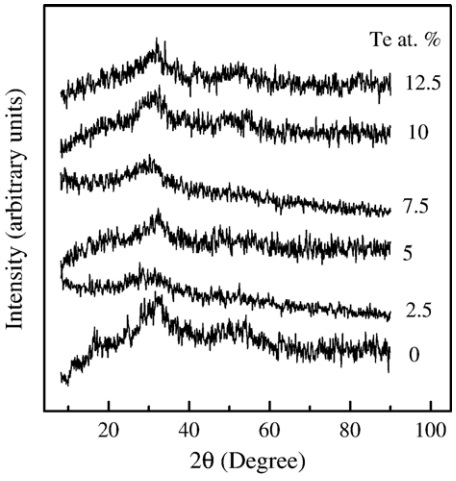

Fig. 1. X-ray diffraction patterns of the $(As_{30}Sb_{15}Se_{55})_{100-x}Te_x$ thin films.

* Corresponding author. Fax: +20 882365432.
E-mail address: Kamalaly2001@yahoo.com (K.A. Aly).

0040-6090/$ - see front matter © 2006 Elsevier B.V. All rights reserved.
doi:10.1016/j.tsf.2006.10.118

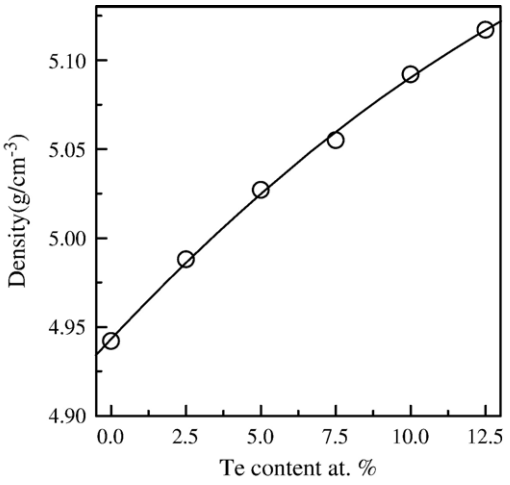

Fig. 2. The compositional dependence of the bulk density of the $(As_{30}Sb_{15}Se_{55})_{100-x}Te_x$ glasses.

made on samples annealed beyond their respective T_g values for ~24 h, under a vacuum of approximately 1.33×10^{-3} Pa.

2. Experimental details

Glasses of the $(As_{30}Sb_{15}Se_{55})_{100-x}Te_x$ (where $x=0.25$, 5, 7.5, 10, and 12.5 at.%) system were prepared from As, Se, Sb and Te elements with high purity (5 N) by the usual melt quench technique. Materials were weighed according to their atomic percentages, charged into clean silica ampoules then sealed under vacuum of $\approx1.33\times10^{-3}$ Pa. The ampoules were put into a furnace at around 1250 K for 24 h. During the heating process the ampoules were shaken several times to maintain their homogeneity, then the ampoules were quenched in ice cooled water to avoid crystallization. The elemental compositions of these glasses were checked by using energy dispersive X-ray analysis and the estimated average precision was about 1.0% in atomic fraction in each element. The amorphous state of the materials was checked using X-ray (Philips type 1710 with Cu as a target and Ni as a filter, $\lambda=1.5418$ Å) diffractometer. The absence of crystalline peaks confirms the glassy state of the prepared samples.

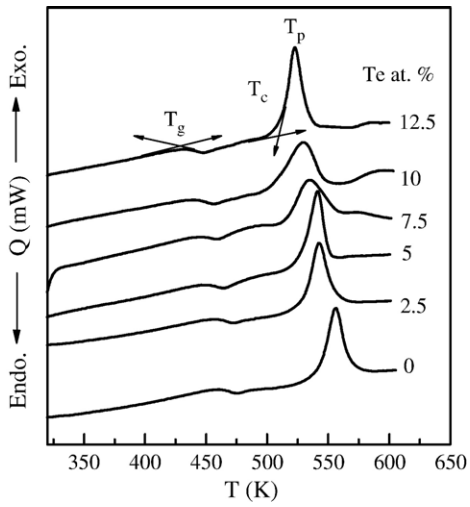

Fig. 3. DSC thermograms of $(As_{30}Sb_{15}Se_{55})_{100-x}Te_x$ glasses recorded at heating rate 10 K/min.

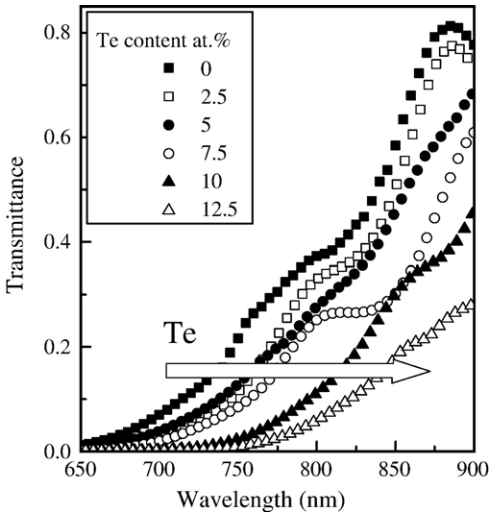

Fig. 4. Transmission spectra of the $(As_{30}Sb_{15}Se_{55})_{100-x}Te_x$ thin films.

Density measurements of the considered samples were made by applying Archimedes method using the hydrostatic weighting in toluene. A single crystal of germanium was used as a reference material for determining the toluene density, ρ_{tol}. The samples density (ρ_s) were determined from the relation

$$\rho_s = \frac{W_{air}}{W_{air}-W_{tol}}\rho_{tol} \quad (1)$$

where W is the weight of the sample. For each composition, the experiment was repeated five times to get the average density of the sample (ρ_s). The thermal behavior was investigated using Shimadzu 50 differential scanning calorimeter (DSC). About 20 mg of each sample in powdered form was sealed in standard aluminum pan and scanned over a temperature range from room temperature to about 600 K at uniform heating rate 10 K/min.

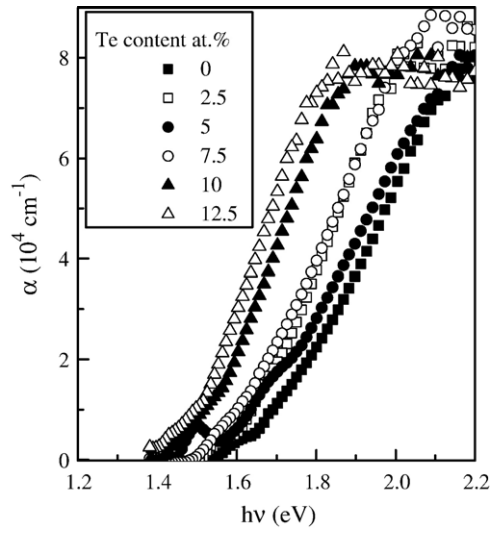

Fig. 5. Photon energy dependence of the absorption coefficient for the $(As_{30}Sb_{15}Se_{55})_{100-x}Te_x$ films.

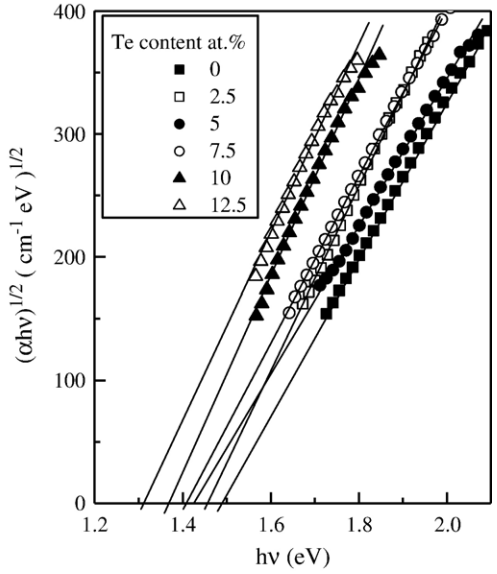

Fig. 6. $(\alpha h\nu)^{1/2}$ vs. $(h\nu)$ plots for the $(As_{30}Sb_{15}Se_{55})_{100-x}Te_x$ thin films.

Thin films were prepared by thermal evaporation of small ingot pieces onto glass substrates (microscope slides). The thermal evaporation process was performed by using a coating (Denton Vacuum 502 A) system, at a pressure of approximately 1.33×10^{-3} Pa. During the deposition process (at normal incidence), the substrates were suitably rotated in order to obtain films of uniform thickness. The thickness of the films lies in the range 900–940 nm. Optical transmittance and reflectance for the thin films have been measured using a double beam (Shimadzu 2101 UV–VIS) spectrophotometer.

3. Results

Fig. 1 shows the X-ray diffraction patterns for the $(As_{30}Sb_{15}Se_{55})_{100-x}Te_x$ thin films. The absence of the diffraction lines in the X-ray patterns indicates that the films have amorphous structures. The compositional dependence of the measured

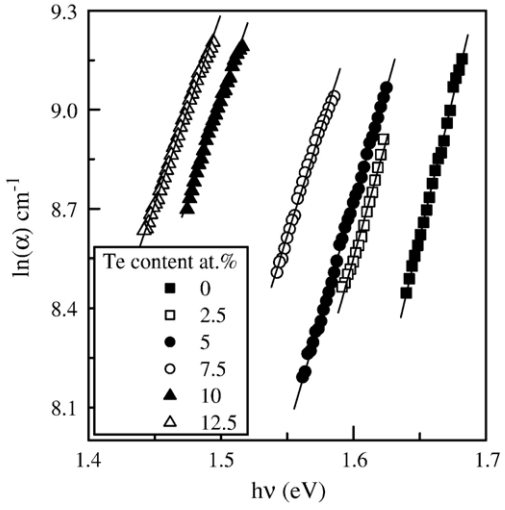

Fig. 7. Relation between ln(α) and (hν) for $(As_{30}Sb_{15}Se_{55})_{100-x}Te_x$ thin films.

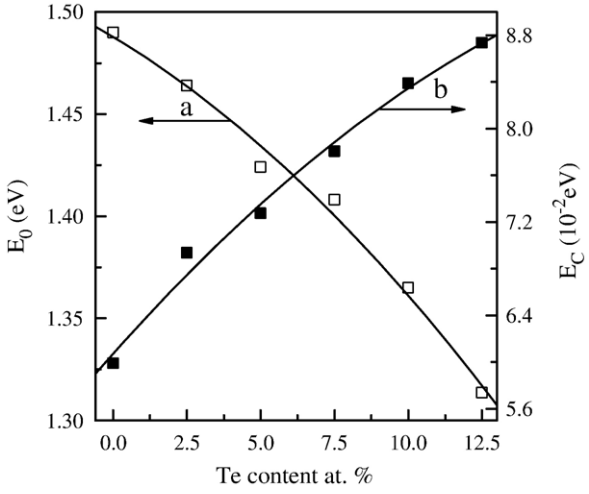

Fig. 8. The variations of E_0 and E_c as a function of Te content for $(As_{30}Sb_{15}Se_{55})_{100-x}Te_x$ thin films.

sample density of the investigated $(As_{30}Sb_{15}Se_{55})_{100-x}Te_x$ glasses is shown in Fig. 2.

Fig. 3 shows the DSC thermograms of amorphous $(As_{30}Sb_{15}Se_{55})_{100-x}Te_x$ chalcogenide glasses recorded at heating rate 10 K/min. This figure shows that there is a very small single endothermic peak. This peak is attributed to the glass transition temperature range which represents the strength or rigidity of the glass structure. Also there is an exothermic peak originating from the amorphous-crystalline transformation. The exo peak has two characteristic points: the first point is the onset temperature of crystallization (T_c) and the second is the peak temperature of crystallization (T_p). It can be seen from Fig. 3 that T_p and $(\Delta T=T_c-T_g)$, which represents that, both the glass transition temperature T_g and the thermal stability ΔT of the glasses, decreases with increasing Te content.

Transmission spectra corresponding to the amorphous $(As_{30}Sb_{15}Se_{55})_{100-x}Te_x$ thin films are plotted in Fig. 4, showing a clear red shift of the interference-free region with increasing Te content. Values of the absorption coefficient (α) for the studied films were calculated from the transmittance T and reflectance R [14,15] using the equation

$$\alpha=\frac{1}{d}\ln\left[\frac{(1-R)^2+\left[(1-R)^4+4R^2T^2\right]^{1/2}}{2T}\right] \quad (2)$$

where d is the thickness of the thin film.

Fig. 5 shows the variation of the absorption coefficient as a function of Te content of $(As_{30}Sb_{15}Se_{55})_{100-x}Te_x$ thin films. As

Table 1
The physical parameters of the constituent elements

Property	As	Se	Sb	Te
Energy gap (eV) [26]	1.15	1.95	0.15	0.65
Density (g/cc) [24]	4.70	4.28	5.3	6.24
Coordination number [19]	3	2	3	2
H_s (kcal/g tom) [21,22]	69.0	49.4	62.0	46
Electronegativity [27]	2.18	2.55	2.05	2.1
Bond energy (kJ mol^{-1}) [33]	32.10	44.04	30.22	33

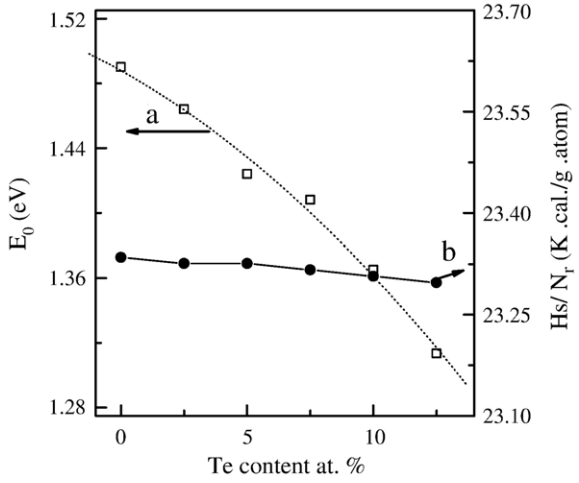

Fig. 9. The optical band gab E_0 and the ratio Hs/Nr as a function of Te content for $(As_{30}Sb_{15}Se_{55})_{100-x}Te_x$ thin films.

shown in this figure the absorption coefficient increases (red shift of the optical absorption edge) with increasing Te content. According to Tauc's relation [16,17] for higher values of the absorption coefficient ($\alpha > 10^4$ cm^{-1}) the allowed non-direct transition, the photon energy dependence of the absorption coefficient can be described by

$$(\alpha h\nu)^{1/2} = B(h\nu - E_0) \tag{3}$$

where B is a parameter that depends on the transition probability and E_0 is the optical energy gap. In the low absorption region ($\alpha < 10^4$ cm^{-1}), the absorption coefficient α shows an exponential dependence on photon energy, hν, and obeys the Urbach relation [18]

$$\ln(\alpha) = \ln(\alpha_0) + (h\nu/E_c) \tag{4}$$

where α_0 is a constant and E_c is the Urbach energy (the width of the band tail of the localized states in the band gap).

Fig. 6 is a typical best fit of $(\alpha h\nu)^{1/2}$ vs. photon energy (hν) for the $(As_{30}Sb_{15}Se_{55})_{100-x}Te_x$ thin films. The intercepts of the straight lines with the photon energy axis give the values of the optical band gap (E_0). Fig. 7 represents the relation between ln (α) vs. (hν). This figure demonstrates that the exponential behaviour of the absorption edge, for Eq. (4) is satisfied. Fig. 8 (a, b) represents the E_0 and E_c values as a function of Te content, It can be noticed that the values of E_0 decrease while E_c increase as Te content increases.

Table 1 shows some physical parameters of the constituent elements that can be used to calculate the different composition parameters such as the average heat of atomization H_s, the cohesive energy CE, and the average coordination number N_r. Finally, Fig. 9(a, b) represents the E_0 and H_s/N_r of $(As_{30}Sb_{15}Se_{55})_{100-x}Te_x$ films as a function of Te content at.%. The obtained values of E_0, E_c and H_s different compositions are listed in Table 2.

4. Discussion

Addition of Te on to $(As_{30}Sb_{15}Se_{55})_{100-x}Te_x$ glasses results in a monotonic increase in the density of these glasses. The measured ρ_S value for the $As_{30}Se_{55}Sb_{15}$ ($x=0$) sample (4.942 g/cm^{-3}) which is in good agreement with that reported previously by Giridhar and Mahadevan [4]. It is known that the density change is related to the change in the atomic weight and the atomic volume of the elements constituting the system. The atomic weights of the As, Se, Sb and Te are 74.92, 78.7, 121.75 and 127.6 respectively, and their respective atomic radii are 1.18, 1.14, 1.36 and 1.6 Å [19–21]. This behavior was expected because the density of Te is the highest one (see Table 1).

Ioffe and Regel [22] suggested that the bonding character in the nearest-neighbour region, which means the coordination number N_r, characterizes the electronic properties of semiconducting materials. The average coordination number N_r in our samples is defined by [23]

$$N_r = 2X\mathrm{Se} + 3X\mathrm{As} + 3X\mathrm{Sb} + 2X\mathrm{Te}. \tag{5}$$

Where X is the mole fraction. Determination of N_r allows the estimation of the number of constraints N_s. This parameter is closely related to the glass-transition temperature and its related properties. For a material with coordination number N_r, N_s can be expressed as the sum of the radial and angular valence force constraints [24],

$$N_s = \frac{N_r}{2} + 2(N_r - 3). \tag{6}$$

The calculated data of N_r and N_s of the $(As_{30}Sb_{15}Se_{55})_{100-x}Te_x$ system are listed in Table 2, using the values of N_r for As, Se, Sb and Te [25] given in Table 1. It can be seen that both N_r as well as N_s decreases with increasing Te content.

Table 2
The calculated and measured density, thermal and optical constants as a function of Te content for $(As_{30}Sb_{15}Se_{55})_{100-x}Te_x$ thin films

Te (at.%)	Density (g/cm^{-3})	T_g (K)	ΔT (K)	N_r*	N_s*	H_s* (kcal/g)	Excess of As–As	CE (eV atom^{-1})	E_0* (eV)	E_0 (eV)	E_c (eV)
0	4.942	462.52	79.92	2.45	0.125	57.17	26	2.205	1.385	1.49	0.059
2.5	4.988	454.92	78.44	2.439	0.097	56.89	30	2.184	1.367	1.464	0.069
5	5.027	450.53	74.33	2.427	0.069	56.61	32	2.165	1.348	1.424	0.072
7.5	5.055	436.05	63.38	2.416	0.041	56.33	38	2.158	1.530	1.408	0.078
10	5.092	432.14	66.98	2.405	0.013	56.05	42	2.135	1.33	1.365	0.083
12.5	5.117	425.07	64.96	2.394	−0.016	55.77	46	2.113	1.293	1.313	0.087

*Calculated values.

According to Pauling [26], the heat of atomization H_s (A–B), at standard temperature and pressure of a binary semiconductor formed from atoms A and B, is the sum of the heat of formation ΔH and the average of the heats of atomization H_s^A and H_s^B that corresponds to the average non-polar bond energy of the two atoms

$$H_s(A-B) = \Delta H + \frac{1}{2}(H_s^A + H_s^B). \quad (7)$$

The first term in Eq. (7) is proportional to the square of the difference between the electronegativities χ_A and χ_B of the two atoms

$$\Delta H \alpha (\chi_A - \chi_B)^2. \quad (8)$$

This idea was extended to quaternary semiconductors compounds by Sadagopan and Gotos [27]. In most cases, the heat of formation of chalcogenide glasses is unknown. In the few materials for which it is known, its value does not exceed 10% of the heat of atomization and therefore can be neglected [28,29]. Hence, H_s (A–B) is given quite well by

$$H_S(A-B) = \frac{1}{2}(H_S^A + H_S^B). \quad (9)$$

The obtained results of the average heat of atomization of $(As_{30}Sb_{15}Se_{55})_{100-x}Te_x$ (where x=0, 2.5, 5, 7.5, 10 and 12.5 at. %) glasses are listed in Table 2, using the values of H_S for As, Se, Sb and Te given in Table 1.

Quaternary semiconductor has hybridized sp^3 orbitals which are split into bonding and antibonding states. In the solid these molecular states are broadened into bands. Thus, in the quaternary semiconductors, the bonding band forms the valence band and the antibonding forms the conduction band. However, in Chalcogenide glasses containing a high concentration of a group VI (Te or Se in our case) element the lone-pair electrons form the top of the valence band and the antibonding band forms the conduction band [30,31]. It is therefore interesting to relate the optical gap with the chemical bond energy, and the parameters we use to specify the bonding are H_s and N. The relation between the energy gap and the average heat of atomization was discussed by Aigrain et al. [32]. According to their study there exists a linear correlation that can be expressed for the semiconductors of the diamond and Zinc-blende structure by

$$\Delta E = a(H_S - B) \quad (10)$$

where a and b are characteristic constants. It is suggested from the above equation that the average heat of atomization is a measure of the cohesive energy and represents the relative bond strengths, which in turn are correlated with the energy gap of isostructural semiconductors.

The bond energies D(A–B) for heteronuclear bonds have been calculated by using the empirical relation

$$D(A-B) = [D(A-A).D(B-B)]^2 + 30(\chi_A - \chi_B)^2 \quad (11)$$

proposed by Pauling [33], where D(A–A) and D(B–B) are the energies of the homonuclear bonds (in units kcal/mol.) [34], χ_A and χ_B are the electronegativity values for the involved atoms [35]. Bonds are formed in the sequence of decreasing bond energy until the available valence of atoms is satisfied [36]. In the present compositions, the Se–Te bonds with the highest possible energy (44.197 kcal mol^{-1}) are expected to occur first. Since the Sb–Se (43.981 kcal mol^{-1}) followed by As–Se (41.706 kcal mol^{-1}) to saturate all available valence of Se. There are still unsatisfied as which must be satisfied by As–As defect homopolar bonds. Based on the chemical bond approach, the bond energies are assumed to be additive. Thus, the cohesive energies (CE) were estimated by summing the bond energies over all the bonds expected in the material. Calculated values of the cohesive energies for all compositions are presented in Table 2. These results indicate that, the cohesive energies of these glasses show a decrease with increasing Te content. Therefore, it can be concluded that the decrease of E_0 with increasing Te (Fig. 8(a)) content is most probably due to the reduction of the average stabilization energy by Te content. It should be mentioned that the approach of the chemical bond neglects dangling bond and other valence defects as a first approximation. Also van der Walls interactions are neglected, which can provide a means for further stabilization by the formation of much weaker links than regular covalent bonds. In connection with the values of the tail width, E_c, it is seen that, the increase of Te content (i.e. decrease in CE) leads to increase of E_c (see Fig. 8(b)). The increase of CE implies higher bonding strength, i.e. high E_0, and this means lower defect bonds, which reduce the band tail width Fig. 8(a, b).

It was found that the variation of energy gap (E_0) with composition in amorphous quaternary alloys can be described [28] by the following simple relation:

$$E_{0(AB)}(Y) = YE_{0A} + (1-y)E_{0B} \quad (12)$$

where Y is the volume fraction of element, A and E_{0A} and E_{0B} are the optical gaps for elements A and B, respectively. Calculations of E_0 based on the above equation for the present $(As_{30}Sb_{15}Se_{55})_{100-x}Te_x$ alloys are tabulated in Table 2.

The effect of Te content on the optical gap E_0 and the Urbach energy E_c for $(As_{30}Sb_{15}Se_{55})_{100-x}Te_x$ is shown in (Fig. 8(a) solid line), from which one can observe that, the decrease in E_0 with increasing Te content. This relation can be described by an empirical formula as follows,

$$E_0 = 1.49332 + 0.01792x - 0.0003228x^2, \quad (13)$$

and the increase in E_c with increasing Te content can be described by the empirical relation (Fig. 8(b) solid line),

$$E_e = 0.0607 + 0.00286x - 0.0000582x^2 \quad (14)$$

where x is the Te content (at.%). The value of the optical gap of $As_{30}Sb_{15}Se_{55}$ (x=0) specimen is equal to 1.49 eV, which is in good agreement with that given by Mathew and Philip Pramana [37]. The decrease in E_0 of amorphous films can be explained by the increased tailing of the band tails in the gap [38] from Fig. 8(a, b). It can be noticed that the values of E_c increase as Te content increases. The Tauc's model [39] based on electronic transitions between localized states in the band edge tails may well be valid for such systems.

Hurst and Davis [40] explained these results by suggesting that when the bond energies in the alloy are not very different, the increase in disorder associated with deviation from stoichiometry will tend to push the mobility edges further into the bands, thereby decreasing E_0. Furthermore, comparing E_0 with H_s given in Table 2, we can find an increase in E_0 with H_s with the increasing Te content of our $(As_{30}Sb_{15}Se_{55})_{100-x}Te_x$ system. But according to Refs. [30,31], E_0 for over constrained materials with higher connectivity, $4 \geq N_r \geq 3$, depends more strongly on H_s than for glasses with lower connectivity, $3 \geq N_r \geq 2$. This result suggests that the parameter H_s/N_r has a very small effect on E_0 which was confirmed in our study (see Fig. 9(a, b)).

5. Conclusions

Addition of Te at the expense of Se, As (Sb) results in the increase of density of the bulk $(As_{30}Sb_{15}Se_{55})_{100-x}Te_x$ alloy while both of the thermal stability, glass transition temperature, the average heat of atomization and the cohesive energy decreases by increasing Te content. Non-direct electronic transition is mainly responsible for the photon absorption inside the investigated films. The optical band gap of the $(As_{30}Sb_{15}Se_{55})_{100-x}Te_x$ films decreases while the width of localized states increases with the increase in Te content.

References

[1] A.R. Hilton, D.J. Hayes, M.D. Rechitin, J. Non-Cryst. Solids 7 (1975) 319.
[2] J.A. Savage, J. Non-Cryst. Solids 47 (1982) 101.
[3] S.M. El-Sayed, G.A.M. Amin, Vacuum 62 (2001) 353.
[4] A. Giridhar, S. Mahadevan, J. Non-Cryst. Solids 51 (1982) 305.
[5] H. Sakata, N. Nakao, J. Non-Cryst. Solids 163 (1993) 236.
[6] E. Akat, G. Aktas, Philos. Mag., B 81 (7) (2001) 689.
[7] Y. Sawan, F.G. Wakim, M. El-Gabaly, M.K. El-Rayess, J. Non-Cryst. Solids 41 (1980) 319.
[8] C. Corredor, I. Quiroga, J. Vazquez, J. Galdon, P. Villares, R. Jimenez Garay, Mater. Lett. 42 (2000) 229.
[9] P.L. Lopez-Alemany, J. Vazquez, P. Villares, R. Jimenez-Garay, J. Mater. Process. Technol. 143–144 (2003) 512.
[10] J. Vazquez, C. Wagner, P. Villares, R. Jimenez-Garay, J. Non-Cryst. Solids 235–237 (1998) 548.
[11] P.L. Lopez-Alemany, J. Vazquez, P. Villares, R. Jimenez-Garay, Thermochim. Acta 374 (2001) 73.
[12] J.A. Savage, J. Non-Cryst. Solids 47 (1982) 101.
[13] M. Kastner, Phys. Rev. Lett. 28 (1972) 355.
[14] A.A. Othman, M.A. Osman, H.H. Amer, A. Dahshan, Thin Solid Films 457 (2004) 253.
[15] A.A. Othman, H.H. Amer, M.A. Osman, A. Dahshan, Radiat. Eff. Defects Solids 159 (2004) 659.
[16] E.A. Davis, N.F. Mott, Philos. Mag. 22 (1970) 903.
[17] H. Fritzsche, Philos. Mag., B 68 (1993) 561.
[18] F. Urbach, Phys. Rev. 92 (1953) 1324.
[19] M. Fadel, Vacuum 48 (1997) 73.
[20] M. Fadel, Vacuum 52 (1999) 277.
[21] M.A. Sidkey, R. E1 Mallawany, R.I. Nakhla, A. Abd E1-Moneim, J. Non-Cryst. Solids 215 (1997) 75.
[22] A.F. Ioffe, A.R. Regel, Prog. Semicond. 4 (1960) 239.
[23] N. Yamaguchi, Philos. Mag. 51 (1985) 651.
[24] J.C. Phillips, M.F. Thorpe, Solid State Commun. 53 (1985) 699.
[25] L. Tichy, H. Ticha, J. Non-Cryst. Solids 189 (1995) 141.
[26] L. Pauling, J. Phys. Chem. 58 (1954) 662.
[27] V. Sadagopan, H.C. Gotos, Solid-State Electron. 8 (1965) 529.
[28] S.S. Fouad, Vacuum 52 (1999) 505.
[29] S.S. Fouad, A.H. Ammar, M. Abo-Ghazala, Physica B 229 (1997) 249.
[30] M. Kastner, Phys. Rev. Lett. 28 (1972) 355.
[31] M. Kastner, Phys. Rev., B 7 (1973) 5237.
[32] C. Benoit, P. Aigrain, M. Balkanski, Selected Constants Relative to Semiconductors, Pergamon Press, New York, 1961.
[33] J. Pauling, Nature of the Chemical Bond Ithaca, Cornell University Press, New York, 1960.
[34] L. Tichy, A. Triska, H. Ticha, M. Frumar, J. Klikorka, Solid State Commun. 41 (1982) 751.
[35] J. Bicermo, S.R. Ovshinsky, J. Non-Cryst. Solids 74 (1985) 75.
[36] B. Jozef, O. Stanford, S. Mahadevan, A. Gridhar, A.K. Singh, J. Non-Cryst. Solids 74 (1985) 75.
[37] G. Mathew, J. Philip Pramana, Mater. Chem. Phys. 60 (1999) 231.
[38] P.P. Nagel, L. Tichy, A. Triska, H. Ticha, J. Non-Cryst. Solids 59/60 (1983) 1015.
[39] J. Tauc, in: F. Abeles (Ed.), The Optical Properties of Solids, North Holland, Amsterdam, 1970, p. 227.
[40] Ch. Hurst, E.A. Davis, in: J. Stuke, W. Brenig (Eds.), Amorphous and Liquid Semiconductors, Taylor and Francis, London, 1974, p. 349.